# A Model-Independent Approach to Assigning Bacteriorhodopsin's Intramolecular Reactions to Photocycle Intermediates

Benedikt Heßling, Georg Souvignier, and Klaus Gerwert

Max-Planck-Institut für Molekulare Physiologie, Dortmund, Germany

ABSTRACT By using factor analysis and decomposition, bacteriorhodopsin's intramolecular reactions have been assigned to photocycle intermediates. Independent of specific kinetic models, the pure BR-L, BR-M, BR-N, and BR-O difference spectra were calculated by analyzing simultaneously two different measurements in the visible and infrared spectral region performed at pH 6.5, 298 K, 1 M KCl, and pH 7.5, 288 K, 1 M KCl. Even though after M formation L, M, N, and O intermediates kinetically overlap under physiological conditions, their pure spectra have been separated by this analysis in contrast to other approaches at which unphysiological conditions or mutants have been used or specific photocycle models have been assumed. The results now provide a set reference spectra for further studies. The following conclusions for physiologically relevant reactions are drawn: (a) the catalytic proton release binding site, asp 85, is protonated in the L to M transition and remains protonated in the intermediates N and O; (b) the catalytic proton uptake binding site asp 96 is deprotonated in the M to N transition and already reprotonated in the N to O transition; (c) proton transfer between asp 96 and the Schiff base is facilitated by backbone movements of a few peptide carbonyl groups in the M to N transition.

## INTRODUCTION

A key element in the understanding of the details of bacteriorhodopsin's (bR) proton pump mechanism is the assignment of intramolecular reactions to specific photocycle intermediates (for a recent review see Lanyi, 1992). The chromophore reactions, the protonation changes of side groups, and the structural backbone change can be described by the same set of apparent rate constants (Gerwert et al., 1990b; Souvignier and Gerwert, 1992). Unfortunately, these experimentally accessible apparent rate constants are not necessarily simply related to intrinsic rate constants describing directly the photocycle reactions. Due to the biphasic decay of at least the intermediate M, an unidirectional photocycle must be excluded (Xie et al., 1987). This implies that the number of apparent rate constants deduced from exponential fit calculations of the absorbance changes is smaller than the number of intrinsic rate constants describing directly the photocycle reactions. As a consequence, photocycle modeling is an experimentally underdetermined problem, and the derived intermediate spectra are model dependent. A large number of photocycle models are proposed in which the intermediates K, L, M, N, and O are differently connected (for a literature survey see Váró and Lanyi, 1990a). These models vary between two extremes: parallel photocycles originating from different $BR_i$ ground states via $K_i$, $L_i$, $M_i$, $N_i$, and $O_i$ and linear photocycles with significant back-reactions between K, L, M, N, and O (Lozier et al., 1975; Hanamoto et al., 1984; Dancshazy et al., 1988; Diller and Stockburger, 1988; Fodor et al., 1988; Kouyama et al., 1988; Chernavskii et al., 1989; Ames et al., 1990; Váró and Lanyi,

1991b). Here we face a fundamental problem in the analysis of molecular reaction kinetics.

To overcome this dilemma, an alternative approach is performed. Based on the measured absorbance difference spectra, which consist of intermediate mixtures at each time of the reaction, the physiologically relevant pure BR-L, BR-M, BR-N, and BR-O intermediate difference spectra are extracted by a mathematical approach called *factor analysis and decomposition* (Malinowski, 1980) and is in principle an extension of singular value decomposition (SVD) (Henry and Hofrichter, 1992). In particular, the intermediates N and O appear almost simultaneously in the M decay under physiological conditions, and the measured difference spectra do not allow a clear-cut assignment of the reactions to N or O (Souvignier and Gerwert, 1992). The approach yields the minimal number of kinetically and spectrally distinct pure intermediates. Those intermediates that are not well separated may still be merged. Restrictions in the calculations are given only for a few well-known specific bands of the respective pure intermediate spectra, but no assumption on the photocycle reactions is made. The idea of factor analysis and its mathematical background is explained (Heßling et al., 1992). The method of decomposition into pure difference spectra differs from those described by Hofrichter et al. (1989), Chen and Braiman (1991), and Váró and Lanyi (1990b). The approach is applied simultaneously to absorbance difference spectra in the visible and infrared spectral region. Based on this analysis, we are now able to assign in a model-independent manner the intramolecular reactions to specific intermediates. The implications of the results for the pump mechanism are discussed.

## MATERIALS AND METHODS

For the details of sample preparation, apparatus, data acquisition, and the global fit procedure, see Souvignier and Gerwert (1992).

In global fit analysis the absorbance changes $\Delta A$ in the visible and infrared are analyzed with sums of $n_r$ exponentials with apparent rate constants $k_l$ and amplitudes $a_l$.

$$\Delta A(v, t) = \sum_{l=1}^{n_r} a_l(v)e^{-k_l t} + a_0(v).$$

In this analysis, the weighted sum of squared differences $f$ between the fit with $n_r$ rate constants $k_l$ and data points at $n_w$ measured wavelengths $v_i$ and $n_t$ time $t_j$ is minimized:

$$f = \sum_{i=1}^{n_w} \sum_{j=1}^{n_t} (w_{ij})^2(\Delta A_{measured}(v_i, t_j) - \sum_{l=1}^{n_r} a_l(v_i)e^{-k_l t_j} + a_0(v_i))^2.$$

In contrast, in factor analysis and decomposition the absorbance changes are described as a product of the pure intermediate difference spectra and their respective time course. The absorbance changes $\Delta A_{ij}$ during a photocycle of $l$ involved intermediates are described by the following $n_w$ times $n_t$ equations:

$$\Delta A_{ij} = de_{ik}c_{kj}$$

where $n_w$ is the number of measured wavelengths; $n_t$ is the number of measured spectra; $\Delta A_{ij}$ is absorbance changes at time $t_j$ and wavelength $v_i$; $d$ is the thickness of the sample; $c_{kj}$ is the concentration of the intermediate $k$ at the time $t_j$; $e_{ik}$ is the difference of extinction coefficient between the pure intermediate $k$ and $BR_{570}$ at wavelength $v_i$; or in matrix form:

$$[A] = [E][C].$$

The $i$th row of matrix $[A]$ represents the time dependence of absorbance changes at wavelength $v_i$, and the $j$th column can be read as the absorbance spectrum at the time $t_j$. Although we know $[A]$ within experimental error the elements of $[E]$ and $[C]$ are unknown. Starting from the original data $[A]$, a matrix $[Z]$, called the covariance matrix, is calculated. With the help of standard mathematical techniques $[Z]$ is decomposed into a set of "abstract" factors $[E]$ and $[C]$, which, when multiplied, reproduce the original data (see Fig. 1). These factors $[E]$ and $[C]$ have a priori no physical meaning, but they show the minimum number of intermediates that describe the absorbance changes without any specific assumption on the photocycle reaction mechanism. In order to give physically meaningful matrices, they are transformed into real factors in an iterative process under weak restrictions on the intermediates spectral shape. The real factors represent the pure intermediates.

$[Z]$ is constructed by premultiplying the data matrix $[A]$ by its transpose

$$[Z] = [A]^T[A].$$

With the help of numerical methods a matrix $[Q]$ can be found that diagonalizes $[Z]$ such that

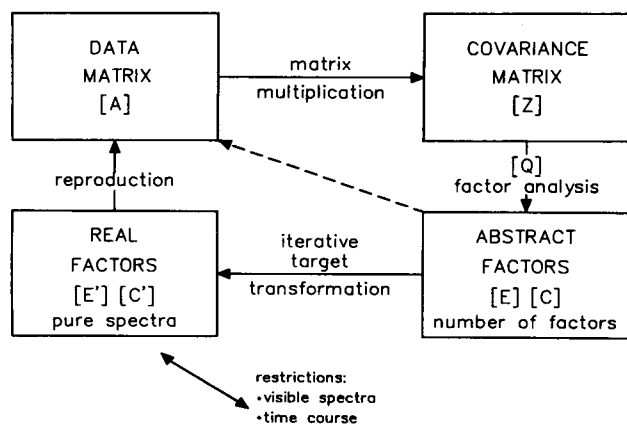$$[Q]^{-1}[Z][Q] = [\lambda_j \delta_{jk}] = [\lambda].$$



FIGURE 1   Scheme of factor analysis and decomposition.

Here $\delta_{jk}$ is the Kronecker delta and $\lambda_j$ is an eigenvalue of the set of equations

$$[Z]Q_j = \lambda_j Q_j.$$

$Q_j$ is the $j$th column of matrix $[Q]$. We showed that the transpose of matrix $[Q]$, which diagonalizes the covariance matrix $[Z]$, represents the matrix $[C]$, and its rows form a set of orthonormal eigenvectors (Malinowski, 1980; Heßling et al., 1992). Multiplying the calculated matrices $[E]$ and $[C]$ we can reproduce the data matrix via a short circuit (Fig. 1). Up to this stage of factor analysis the original data are exactly described by a set of mutually orthonormal eigenvectors. Due to experimental error, however, the number of eigenvectors found does not depend on the number of involved intermediates but on the dimension of matrix $[A]$. Without error the number of eigenvalues unequal to zero would represent directly the number of distinct intermediates. Each successive eigenvector accounts for the greatest possible variance in the data (a formal definition is given in Malinowski, 1980). The most important eigenvector associated with the greatest eigenvalue is oriented in a factor space, constituted by all eigenvectors, so as to account for the maximum possible variance. It defines the best one-factor model. Since the least important eigenvectors associated with the smallest eigenvalues in practice regenerate the experimental error we recalculate the data matrix using only the most important eigenvector $Q_1$ to obtain $E_1$ and $C_1$. We continue adding eigenvectors associated with the largest eigenvalues, sequentially, until the product reproduces the data within error:

$$[E_1 E_2 \dots E_n] \begin{bmatrix} C_1 \\ C_2 \\ \dots \\ C_n \end{bmatrix} = [E^*][C^*] = [A^*] \cong [A].$$

The minimum number of eigenvectors $n$ yielded in this step represents the number of factors (i.e., intermediates) that describe the data within the error without any assumption regarding the reaction kinetics. These abstract eigenvectors have no physical meaning. The physically meaningful real factors, that is, the pure intermediate difference spectra, are not necessarily orthonormal to each other but are linear combinations of the abstract factors. Up to this stage the SVD and this approach should yield the same abstract factors. Using SVD as a matrix rank reduction algorithm, in different applications a specific photocycle model is then assumed to deduce pure intermediate difference spectra (Chen and Braiman, 1991; Lozier et al., 1992). In order to obtain the real factors, that is, the pure intermediate spectra, here a different, iterative procedure is used in the last step. Since the pure intermediate spectra $E_i'$ are linear combinations of the calculated $E_i$,

$$E_i' = a_i E_1 + b_i E_2 + \dots$$

We are seeking a transformation matrix $[T]$ and its inverse $[T]^{-1}$ with the property

$$[A^*] = [E^*][C^*] = [E^*][T][T]^{-1}[C^*] = [E'][C'].$$

In order to search for solutions in such a multidimensional parameter space, recent work (Zimanyi and Lanyi, 1993) showed the applicability of filters in a grid search algorithm. In the studied case, mutated asp 96 asn bacteriorhodopsin, only three base spectra must be examined. For practical reasons this kind of strategy is inadequate for data containing more than three base spectra. Here we proceed in two steps. First we narrow the solution space by orienting the spectral shape of three real factors in the infrared to low-temperature BR-L and BR-M difference spectra and a BR-N measured at high pH. Thus, keeping those coefficients fixed, the solution space can be reduced to a reasonable number of grid points. Those grid points, obeying criteria 1–3 (see below), are used as starting points for the second step. Then, during iteration, all coefficients $a_i$, $b_i$, ... are varied randomly so that

1. The pure difference spectra in the visible (i.e., elements of $[E']$) are similar to generally accepted difference spectra in the literature (Váró and Lanyi, 1991a; Lozier et al., 1992), but deviations are allowed.
2. Positive intermediate concentrations are found (i.e., all elements of $[C']$ are positive).
3. The weighted sum of difference between the input data matrix $[A]$ and recalculated data $[E'][C']$ is minimized.

Even though these restrictions are relatively weak, the iteration converges to a clear minimum.

The analysis described was applied to the absorbance changes of bR from 50 $\mu$s to 700 ms after flash excitation in the infrared measured with stroboscope Fourier Transform Infrared Spectroscopy and 12 wavelengths in the visible spectral range of two different measurements performed at pH 6.5, 298 K, 1 M KCl, and at pH 7.5, 288 K, 1 M KCl. Data were taken with 4 cm$^{-1}$ spectral resolution and 20 $\mu$s time resolution. For factor analysis 250 difference spectra from the measurement at pH 6.5 and 350 difference spectra from the measurement at pH 7.5 are condensed by averaging to 20 difference spectra, respectively, equally spaced on a logarithmic time scale. With 12 wavelengths in the visible (410, 430, 460, 500, 530, 550, 570, 590, 620, 640, 660, 680 nm) and 361 wavenumbers in the infrared (1800–1100 cm$^{-1}$), the input data comprise a 373 $\times$ 40 matrix.

## RESULTS

In order to obtain high-quality pure difference spectra of physiological relevance the analysis is applied to two different measurements performed close to physiological conditions. Application of the analysis to one measurement did not separate N and O spectra satisfactorily. In one experiment performed at pH 6.5, 298 K, and 1 M KCl the O intermediate accumulates during the M decay and in the other performed at pH 7.5 and 288 K the N intermediate dominates (Kouyama et al., 1988; Smith et al., 1983). In particular, the proposed fast equilibrium reaction of microseconds between N and O renders it difficult to assign reactions to the respective intermediates (Chernavskii et al., 1989; Souvignier and Gerwert, 1992). In order to exclude unphysiological reactions, these specific conditions are used even if it seems that under extreme external conditions (pH, temperature) some reactions are better visualized (Smith et al., 1983; Pfefferlé et al., 1991; Ormos et al., 1992). Furthermore, it became clear that data in the visible and infrared spectral region have to be analyzed simultaneously. In the first part of this section, the results of the conventional global multiexponential fit analysis in the visible and infrared spectral region of the two measurements are discussed. This allows a comparison of the conventional approach with the new one. In the following the results of the global fit analysis are discussed in the context of the factor analysis results described later.

### Global Fit Analysis of Visible Absorbance Changes

In Fig. 2, three-dimensional presentations of the two measurements in the visible spectral range are shown. At pH 7.5 (Fig. 2, bottom) the photocycle is slowed down compared to pH 6.5 (Fig. 2, top). The disappeared BR ground state absorption and its reappearance can be followed at 570 nm, the L-decay produces a shoulder at 530 nm, and the M rise and decay can be followed mainly at 410 nm. Comparison of the absorbance changes at 680 nm, indicative of O accumulation,
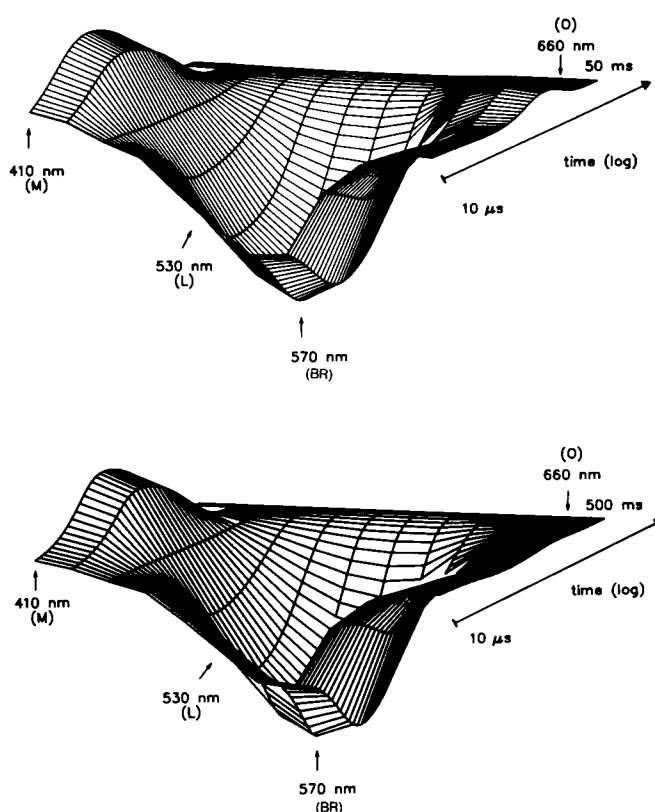


FIGURE 2   Three-dimensional graph of multiexponential fit results of absorbance changes in the visible spectral region during the bacteriorhodopsin photocycle. (a) at pH 6.5, 298 K, 1 M KCl; (b) at pH 7.5, 288 K, 1 M KCl.

shows significant O concentration at pH 6.5 but almost no O accumulation at pH 7.5. Due to the broad overlap of N and BR absorption, the N intermediate cannot be followed in the visible directly (Kouyama et al., 1988). Selected time courses of absorbance changes from Fig. 2 are shown in Fig. 3, as are results of the global fit analysis (Gerwert et al., 1990b; Souvignier and Gerwert, 1992). The absorbance changes represent mainly the time dependence of M (410 nm) and O (680 nm) concentrations. The exponential fit curve and the three dominating apparent rates $k_i$, with their relative contributions, are presented. The absorbance changes are fully described at pH 6.5 with five apparent rates and at pH 7.5 with six in agreement with Xie et al. (1987) and Souvignier and Gerwert (1992). The biphasic M rise is not resolved at pH 6.5. Numbering of rates is in the order of their appearance, that is, their significance in the fit calculation. The L to M reaction is dominated by $k_2$ and the M decay by $k_3$ and $k_4$ (Fig. 3, a and b). The appearance of O is mainly described by $k_4$ (Fig. 3 c). The corresponding amplitude spectra $a_i(\nu_l)$ (i.e., the wavelength dependence of the apparent rates) are given in Fig. 3 (e and f). The relative contributions of the rates to the respective absorbance changes can be followed. In a linear scheme they would already represent the searched-for pure difference spectra, if the intermediates are kinetically well separated. But here they represent mixtures of intermediates. In Fig. 3 (e and f) $k_2$ (and at pH 7.5 $k_5$) describes the
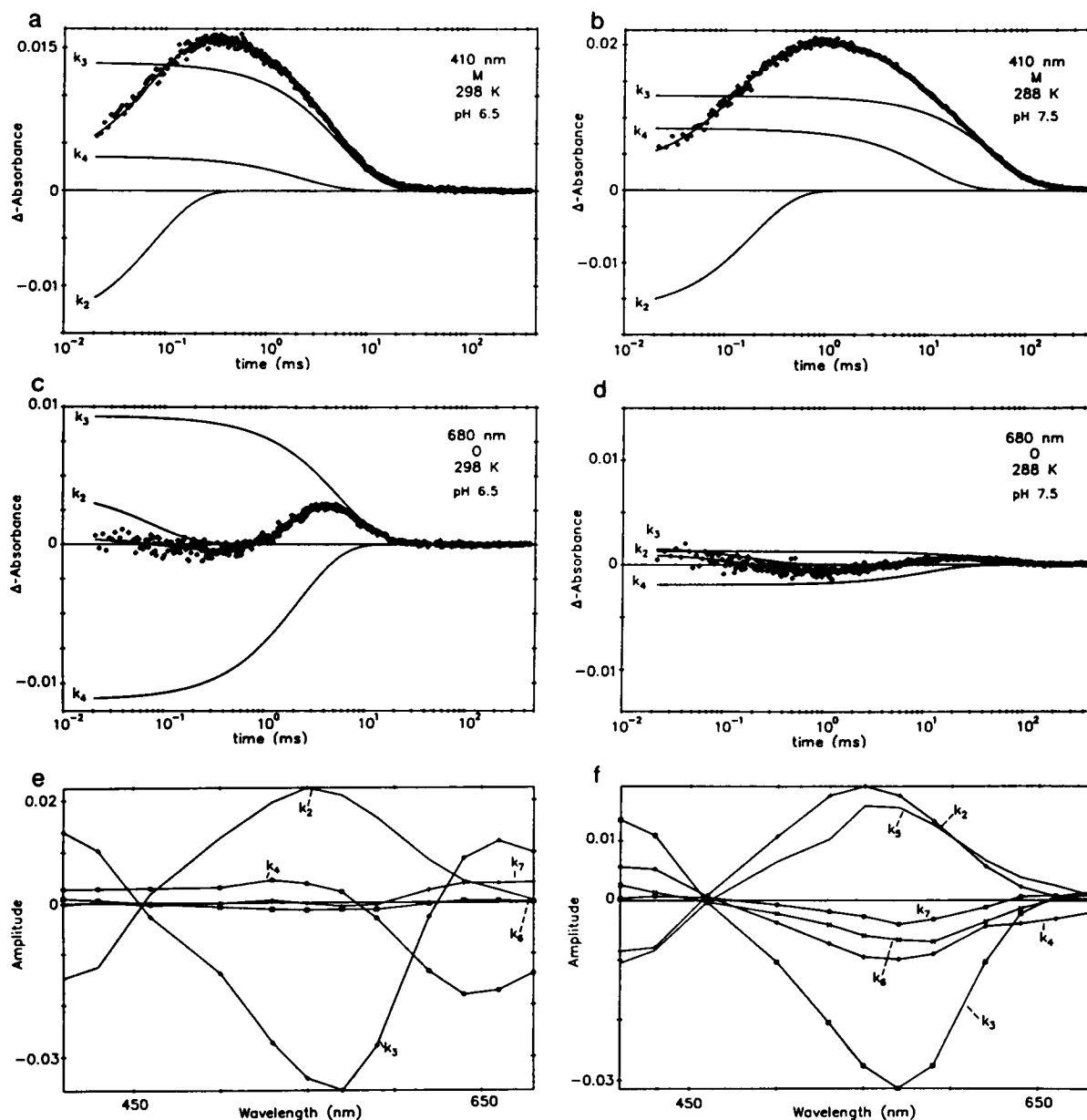
**FIGURE 3** Selected absorbance changes from Fig. 2 with exponential fit curve and the three dominating rates. (*a*) at 410 nm, pH 6.5; (*b*) 410 nm pH 7.5; (*c*) 680 nm, pH 6.5; (*d*) 680 nm, pH 7.5; (*e*) the amplitude spectra of all apparent rates describing the absorbance changes at pH 6.5 with $t_2 = 0.1$ ms, $t_7 = 0.3$ ms, $t_4 = 1.4$ ms, $t_3 = 3.5$ ms, $t_6 = 26.4$ ms (it represents order of appearance in the fit); (*f*) amplitude spectra at pH 7.5 with $t_2 = 0.1$ ms, $t_5 = 0.6$ ms, $t_7 = 1.3$ ms, $t_4 = 4.4$ ms, $t_3 = 24.2$ ms, $t_6 = 75$ ms.

disappearance of L (550 nm) and the appearance of M (410 nm). Rate constant $k_3$ represents at pH 6.5 the M (410 nm) and O (680 nm) decay (Fig. 3 *e*), whereas at pH 7.5 it represents only the M decay (410 nm) (Fig. 3 *f*). At pH 6.5 $k_4$ describes mainly the disappearance of M (410 nm) and the appearance of O (680 nm). At pH 7.5 it reflects the disappearance of M and the appearance of N (around 570 nm). $k_6$ shows wavelength dependence similar to that of $k_3$ but is much smaller. The contribution to M decay is almost negligible at pH 6.5 and significant at pH 7.5. $k_7$ contributes at pH 6.5 to O decay and at pH 7.5 to N appearance. This is in agreement with the conclusion that $k_7$ is con-

nected to the N-O equilibrium reaction (Souvignier and Gerwert, 1992).

## Global Fit Analysis of Infrared Absorbance Changes

In Fig. 4 a three-dimensional presentation of the two measurements in the infrared spectral region are shown (compare Fig. 2, *a* and *b*). The time course of absorbance changes at 1186 cm$^{-1}$ (pH 6.5 and pH 7.5) at 1503 cm$^{-1}$ (pH 6.5) and 1385 cm$^{-1}$ (pH 7.5) is shown in Fig. 5. As for the visible data, the exponential fit curve and the three dominating rates are
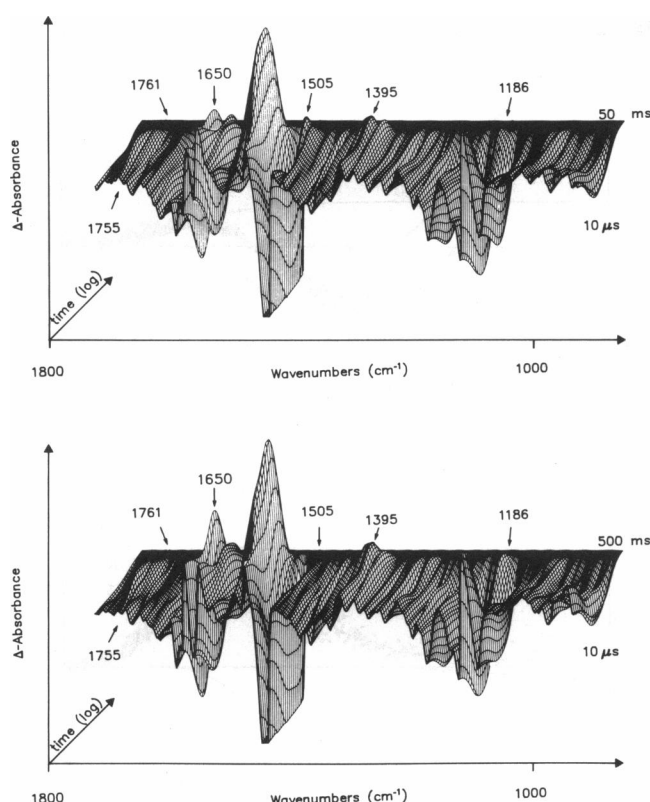
FIGURE 4　Three-dimensional graph of IR absorbance changes between 1800 and 1000 $cm^{-1}$ with 4 $cm^{-1}$ spectral resolution. (*a*) at pH 6.5; (*b*) at pH 7.5.

also given. Appearance of the band at 1186 $cm^{-1}$ (not time resolved) is indicative of all-*trans* to 13-*cis* isomerization (Smith et al., 1984). Its disappearance, dominated by $k_2$, shows the deprotonation of the Schiff base in the L to M transition. Its reappearance, dominated by $k_4$, describes reprotonation of the Schiff base, and its final disappearance, dominated by $k_3$ at pH 6.5 and $k_6$ at pH 7.5, indicates the relaxation of the chromophore configuration to the initial BR ground state (Fig. 5, *a* and *b*). The absorbance change at 1503 $cm^{-1}$ reflects mainly the concentration dependence of the O intermediate (Fig. 5 *c*), as does the absorbance change at 680 nm (Fig. 3 *c*) (Smith et al., 1983). Its rise is dominated by $k_4$, its decay by $k_3$. At 1385 $cm^{-1}$ the N formation can be followed (Fig. 5 *d*) (Souvignier and Gerwert, 1992). Its rise is dominated by $k_4$, as for O, and its decay by $k_6$.

In Fig. 6 the corresponding infrared (IR) amplitude spectra are given. The $k_2$ amplitude spectra representing the L to M reaction agree very well in the two different measurements, indicating their spectral independence of external parameters. In Fig. 6 *a* only the $k_2$ amplitude spectrum of the measurement at pH 7.5 is shown. The characteristic reactions of the L to M transition are reflected: disappearance of the retinal band at 1190 $cm^{-1}$ and 1159 $cm^{-1}$, disappearance of the 1747 $cm^{-1}$, and appearance of the 1762 $cm^{-1}$ asp-carbonyl bands. The $k_3$ amplitude spectrum at pH 7.5 in Fig. 6 *b* represents mainly the M to BR reaction. In Fig. 6 (*c* and *d*) the $k_4$ amplitude spectra are shown. They represent mainly the

M to O reaction at pH 6.5 and the M to N reaction at pH 7.5, respectively. This becomes obvious by comparing the bands at 1507 $cm^{-1}$ and 1171 $cm^{-1}$ in the two different measurements, which are indicative of O formation (Smith et al., 1983). (The amplitude spectra are multiplied by $-1$ for better visualization.) The $k_3$ amplitude spectrum obtained at pH 6.5 reflects mainly the O to BR reaction as indicated at 1505 $cm^{-1}$ and 1173 $cm^{-1}$ (Fig. 6 *e*). At pH 7.5 the M decay is slowed down, and thereby the M and N intermediates are kinetically better separated than M and O at pH 6.5. At pH 7.5 the $k_3$ amplitude spectrum reflects mainly an M to BR reaction (Fig. 6 *b*), whereas the $k_6$ amplitude spectrum mirrors an N to BR reaction (Fig. 6 *f*).

## Factor Analysis and Decomposition

With factor analysis and decomposition, the pure intermediate difference spectra are extracted from the measured absorbance difference spectra representing intermediate mixtures. In the first step the minimum number of spectrally and kinetically different abstract factors describing the absorbance changes are determined (see also scheme in Fig. 1). Up to this stage the same mathematical principles as in SVD are used (Hofrichter et al., 1989; Chen and Braiman, 1991). It is found that four factors are needed to describe absorbance changes during the L to BR reaction pathway (i.e., between 50 $\mu$s and 700 ms within experimental error). Importantly, this was found without the assumption of specific photocycle models and not even with the assumption of first-order reactions. In the iteration the measured absorbance changes at 12 wavelengths in the visible and 361 wavenumbers in the infrared are condensed to 40 difference spectra comprising a 373 × 40 input matrix. As an example one comparison is shown in Fig. 7 *a* between the measured difference spectrum 120 $\mu$s after flash excitation and the calculated difference spectrum with four factors. Three factors do not satisfactorily describe the difference spectrum, whereas adding a fifth factor only reproduces experimental error (data not shown). In the extension of SVD in the next step the real factors (i.e., the pure intermediate difference spectra) are calculated as linear combinations of the four abstract factors in an iterative process. This iteration makes the analysis independent of specific kinetic models. Nevertheless it is assumed that intermediates like L, M, N, and O exist. As an example, the fingerprint region for the same measured difference spectrum is compared with the result of one, two, three, and four real factor analysis. Four real factors satisfactorily describe the data (Fig. 7 *b*). The good description of all measured difference spectra in the visible and infrared with four factors is the first control of the approach. Recently in a similiar approach (Zimanyi and Lanyi, 1993) the asp-96-asn mutant photocycle was analyzed. As discussed in Materials and Methods this is not transferable to the wild type, in which four instead of three intermediates must be examined. In other approaches also starting with SVD specific photocycles are assumed to yield pure intermediate spectra (Hofrichter et al., 1989; Chen and Braiman, 1991).
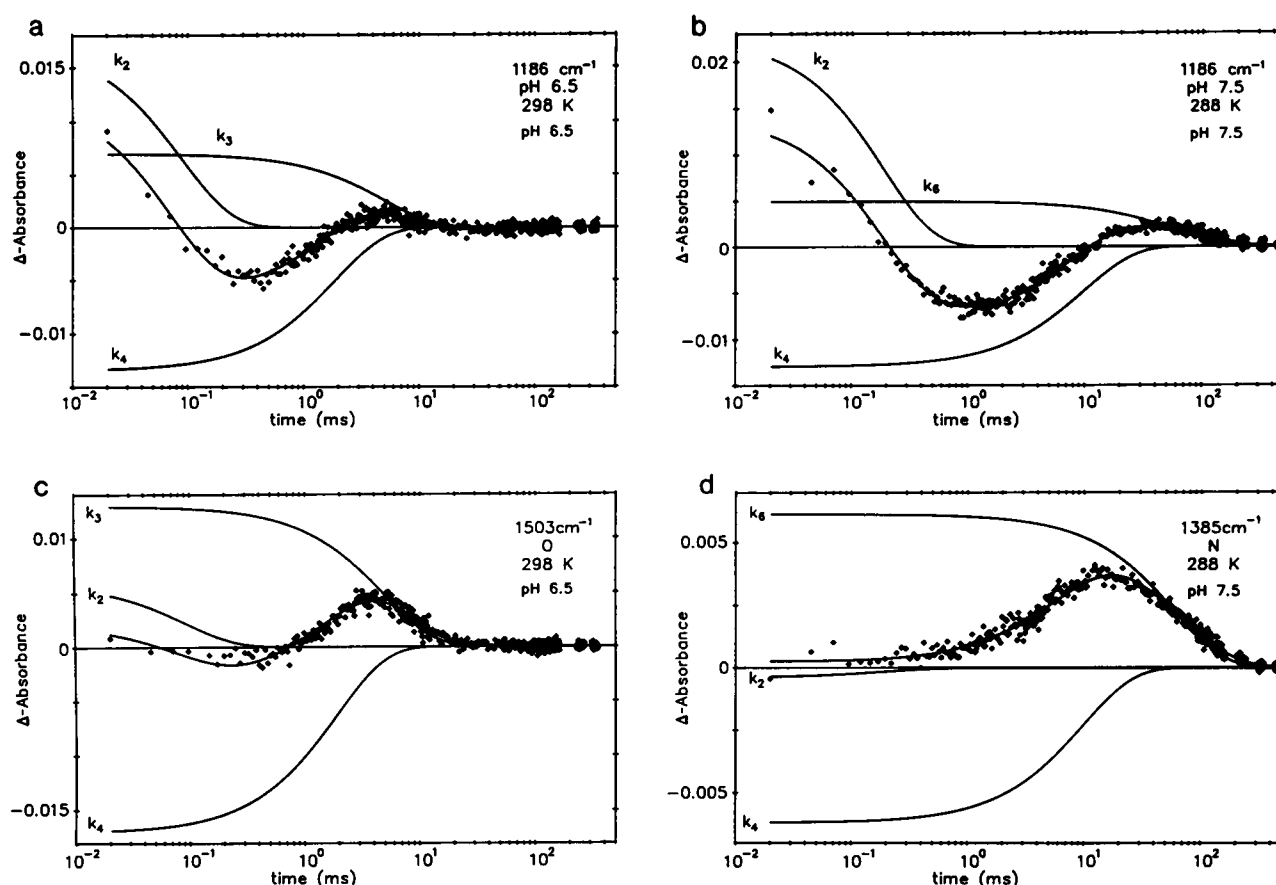
FIGURE 5    Selected absorbance changes from Fig. 4 with exponential fit curve and the three dominating rates. (a) at 1186 cm$^{-1}$, pH 6.5; (b) at 1186 cm$^{-1}$, pH 7.5; (c) at 1503 cm$^{-1}$, pH 6.5; (d) at 1385 cm$^{-1}$, pH 7.5.

## Pure Difference Spectra in the Visible Spectral Range

In Fig. 8, the calculated pure BR-L, BR-M, BR-N, and BR-O difference spectra in the visible spectral range [$E'$] are shown. In general they agree well with difference spectra obtained by model-dependent approaches (Lozier et al., 1992; Váró and Lanyi, 1991a), except that the small amplitude at 410 nm in the BR-N difference spectrum is in full agreement with the results of Lozier et al. (1992) but disagrees with those of Váró and Lanyi (1991a). Nevertheless, the overall general good agreement with the results given by Lozier et al. (1992) and Váró and Lanyi (1991a) can be regarded as a second control of this approach.

A third control is the agreement of the time course of the intermediate concentrations [$C'$] with characteristic absorbance changes of the respective intermediates. In Fig. 9, the time dependence of the L, M, N, and O concentrations as yielded by factor analysis are given for pH 6.5 (Fig. 9, top) and pH 7.5 (Fig. 9, bottom). In addition the curves yielded by multiexponential refitting of the intermediate concentrations are shown. Even though exponential behavior was not assumed in the analysis the same apparent rates are obtained as by global fitting of the measured absorbance changes. As expected, because only four spectrally and kinetically different basic spectra are found, at pH 6.5 the apparent rate $k_6$ and at pH 7.5 the apparent rates $k_5$ and $k_6$ are not revealed

in refitting the concentrations. The L decay and M formation agree well with the absorbance changes at 410 nm at pH 6.5 (compare Fig. 9, top, with Fig. 3 a). At pH 7.5 the time course of the M concentration deviates slightly in the decay as compared to the absorbance change at 410 nm (compare Fig. 9, bottom, with Fig. 3 b). This finding is complementary to the appearance of the small amplitude at 410 nm in the BR-N difference spectrum (Fig. 8). It may indicate that factor analysis describes only an early M, does not resolve a second M, and merges it to N. The O concentration coincides with the absorbance change at 680 nm and 1503 cm$^{-1}$, respectively (compare Fig. 9 with Fig. 3, c and d and Fig. 5 c). The N concentration agrees with the absorbance change at 1385 cm$^{-1}$, which is indicative of N formation (compare Fig. 5 d).

All three controls presented show that the four calculated pure difference spectra describe satisfactorily, within experimental error, the absorbance changes during the photocycle between 50 $\mu$s and 700 ms.

## Pure Difference Spectra in the Infrared Spectral Region

### BR-L

In Fig. 10 the pure BR-L room temperature difference spectrum as yielded by factor analysis (Fig. 10 a) and for comparison the low temperature BR-L difference spectrum taken
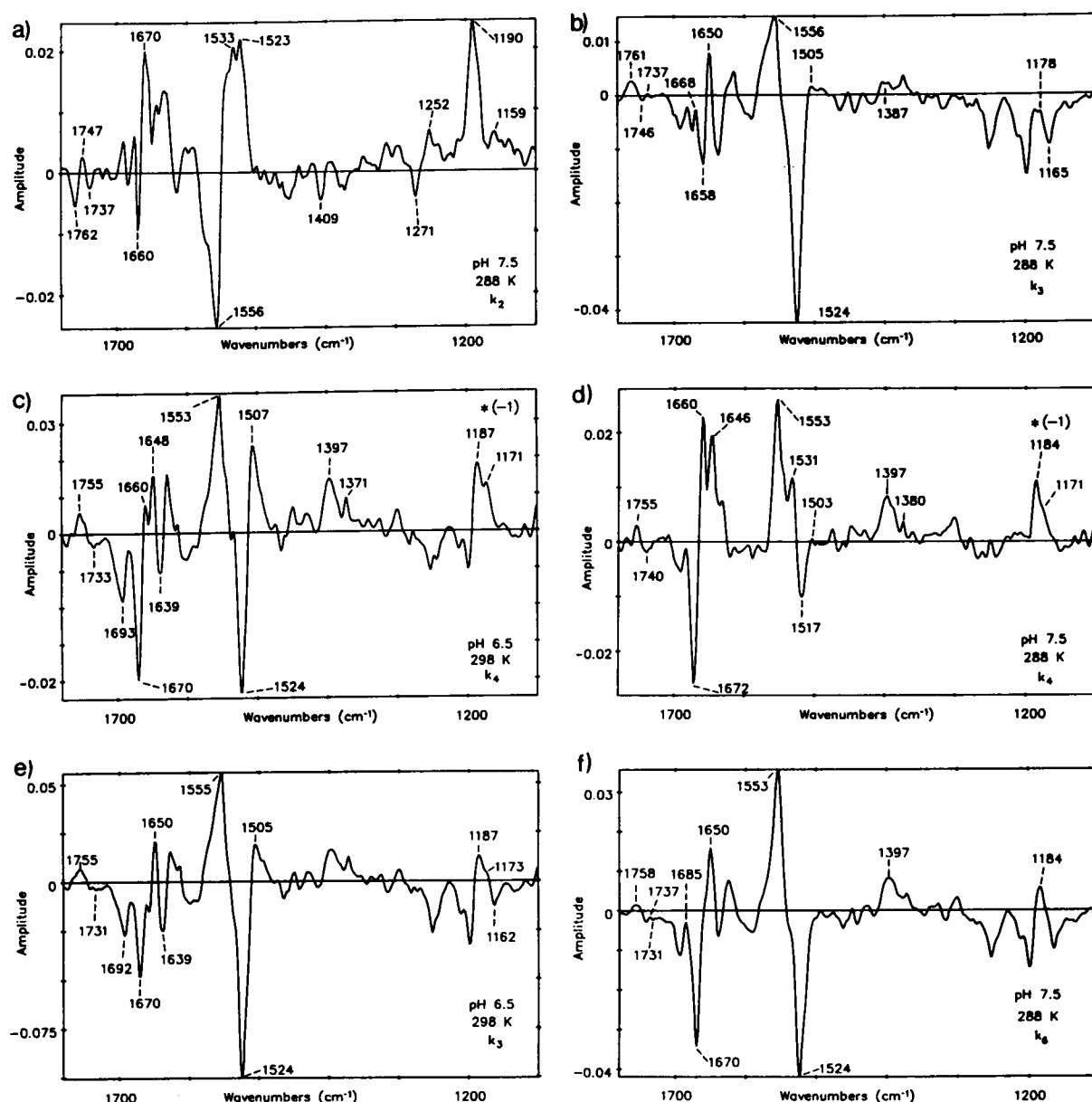
FIGURE 6   IR amplitude spectra. (a) $k_2$ at pH 7.5; (b) $k_3$ at pH 7.5; (c) $k_4$ at pH 6.5; (d) $k_4$ at pH 7.5; (e) $k_3$ at pH 6.5; (f) $k_6$ at pH 7.5.

at 100 K (Fig. 10 b) are shown. In general they agree, but significant deviations are seen in the carbonyl region at 1748, 1712, 1698, 1686, 1679, and 1660 cm$^{-1}$ and minor deviations between 1500 and 1300 cm$^{-1}$. The lack of the shoulder at 1748 cm$^{-1}$ and the additional band at 1712 cm$^{-1}$ are in agreement with earlier time-resolved IR room temperature measurements in this spectral region (Engelhard et al., 1985). The signal-to-noise ratio is significantly increased compared to the results of Chen and Braiman (1991) and Bousche et al. (1991), as can be seen for example by comparison of the amide I region. A prominent band seen at 1300 cm$^{-1}$ in Chen and Braiman (1991) is clearly assigned in our analysis to N, but only a less pronounced band is seen in L. The band seems therefore not to be indicative of asp-96 deprotonation in L (Chen and Braiman, 1991).

## BR-M

In the literature, a confusing variety of BR-M difference spectra in the infrared spectral region is presented, deviating mainly in the fingerprint region at 1180 cm$^{-1}$ and in the amide I/amide II region to each other (Engelhard et al., 1985; Gerwert et al., 1989; Ormos, 1991; Bousche et al., 1991; Fahmy et al., 1992; Maeda et al., 1992; Perkins et al., 1993). The BR-M difference spectrum yielded by factor analysis is shown in Fig. 11 A. No retinal bands of protonated Schiff base intermediates (i.e., positive bands) are observed in the fingerprint region, as indicated, for example, by the decrease at 1180 cm$^{-1}$. Therefore, we conclude that the BR-M difference spectrum in Fig. 11 A is the purest with physiological relevance, and the deviations from published BR-M difference spectra are due to different impurities of L, N, and O,
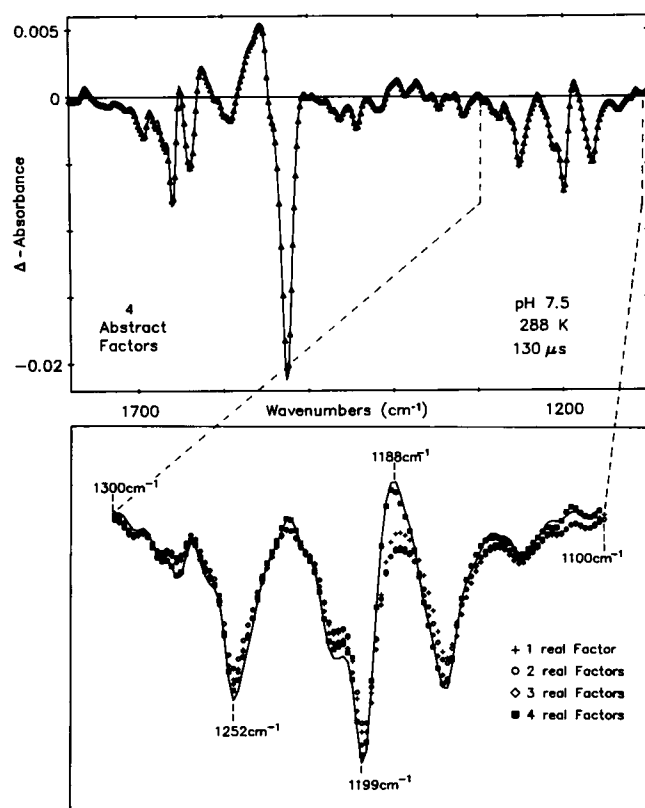
FIGURE 7   IR difference spectrum taken 130 $\mu$s after flash excitation. (*Top*) description of the data by four abstract factors; (*bottom*) description of the absorbance changes in the fingerprint region by 1, 2, 3, and 4 real factors.
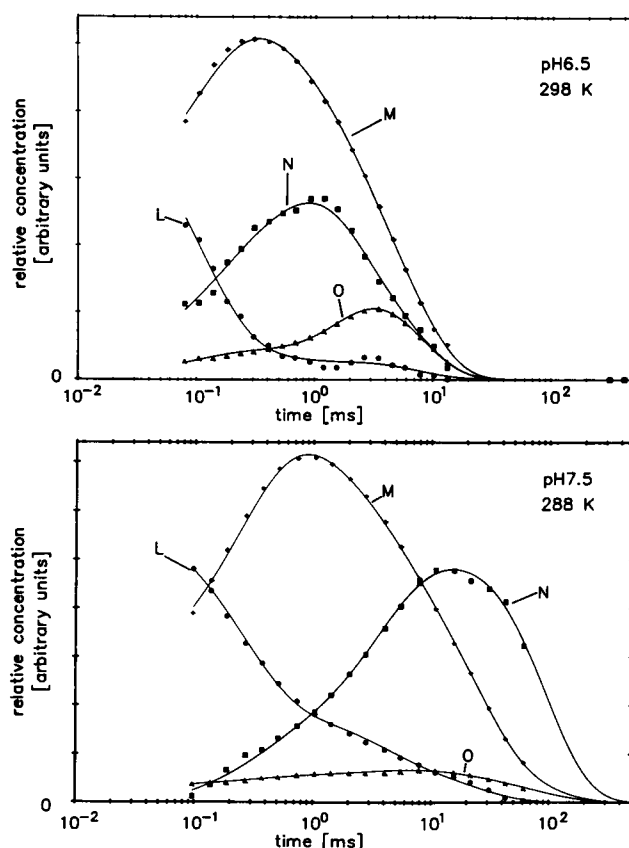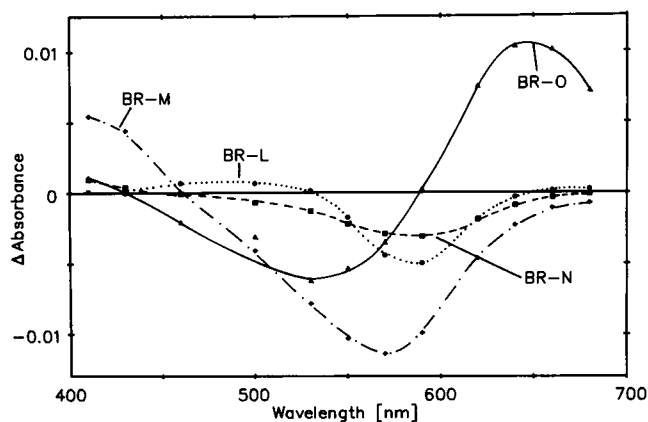


FIGURE 8   Calculated pure intermediate difference spectra in the visible.

depending on the specific pH and temperature used. As now elucidated by factor analysis, the band at 1180 cm is increased in L, N, and O compared to the BR-M difference spectrum shown in Fig. 11 *A*. In addition, an amplitude spectrum of a measurement performed at 220 K is shown. At 220 K two rates describe the M decay. The amplitude spectrum of the faster rate is almost identical to the BR-M difference spectum obtained by factor analysis. The amplitude spectrum of the slower rate is shown in Fig. 11 *B*. It is almost



FIGURE 9   Concentrations of L, M, N, and O in dependence of time as yielded by factor analysis. (*Top*) pH 6.5; (*bottom*) pH 7.5.

identical but deviates at 1180 cm$^{-1}$ and in the amide I region at 1670/1650 cm$^{-1}$.

## BR-N

The pure BR-N difference spectrum as yielded by factor analysis is shown in Fig. 12. It is almost identical to the $k_6$ amplitude spectrum at pH 7.5, which reflects the N to BR reaction (compare Fig. 6 *d*). Furthermore, it agrees nicely with the BR-N difference spectrum obtained at pH 10 (Pfefferlé et al., 1991) and confirms now its relevance for physiological conditions. Characteric spectral features are the shifted asp-carbonyl band at 1755 cm$^{-1}$, the negative band of asp-96 at 1741 cm$^{-1}$, the strong difference band at 1670/1650 cm$^{-1}$, and the strong difference band at 1553/1525 cm$^{-1}$, 1395 cm$^{-1}$, and 1183 cm$^{-1}$. The band at 1183 cm$^{-1}$ indicates the reprotonation of the Schiff base. It is clear now that the shoulder at 1755 cm$^{-1}$ observed in the so-called BR-M difference spectra is due to N impurities.

## BR-O

The pure BR-O difference spectrum is shown in Fig. 13. Characteristic spectral features of O observed in resonance Raman experiments are the ethylenic band at 1507 cm$^{-1}$ and an additional retinal stretching vibration at 1172 cm$^{-1}$ (Smith et al., 1983). The comparison with the $k_3$ amplitude spectrum
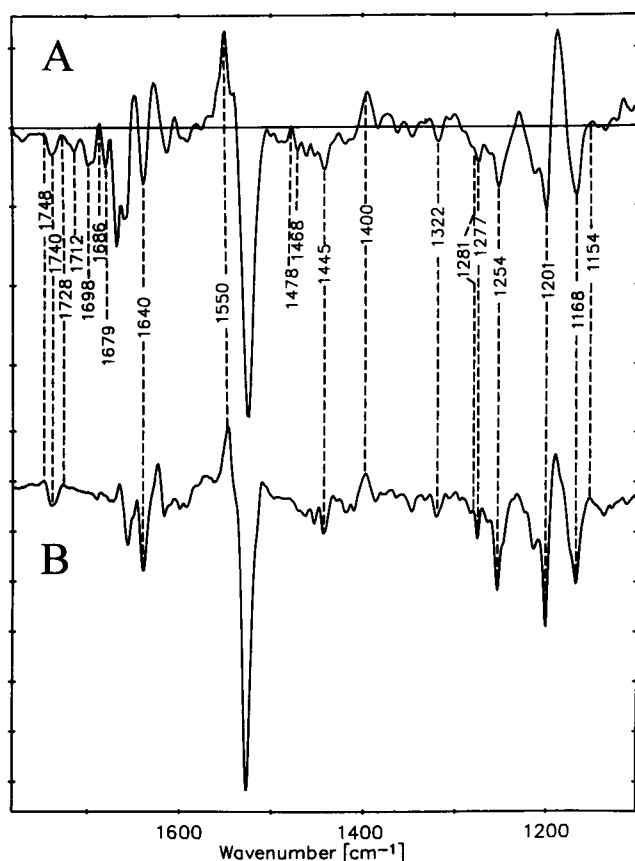
FIGURE 10   (A) pure BR-L difference spectrum of the factor analysis; (B) low-temperature BR-L at 100 K.



FIGURE 11   (a) pure BR-M difference spectrum as yielded by factor analysis; (b) amplitude spectrum of the slower M decay rate at 220 K.

in Fig. 6 e shows that features of O can already be identified in the $k_3$ amplitude spectrum but the pure BR-O difference spectrum is only obtained by factor analysis. This can be seen by comparison of the band at 1505 cm$^{-1}$ in Fig. 6 e and in Fig. 13. It is obvious now that the band at 1740 cm$^{-1}$ indicating asp-96 deprotonation disappears only in N but not in O in agreement with global fit analysis (Souvignier and Gerwert, 1992). The posibility can be excluded that the band at 1733 cm belongs to asp-96 (Gerwert et al., manuscript in preparation).

## DISCUSSION

By factor analysis and decomposition we are now able to present the pure BR-L, BR-M, BR-N, and BR-O difference spectra in the visible and, for the first time, in the infrared spectral region which have physiological relevance. The pure difference spectra are obtained from the simultaneous analysis of two different measurements performed close to physiological conditions at pH 6.5, 292 K, 1 M KCl, and pH 7.5, 287 K, 1 M KCl. At pH 6.5 the O intermediate dominates the M to BR reaction pathway, whereas at pH 7.5 the N is kinetically separated from M decay and accumulates. In contrast to other approaches no assumption on specific photocycle models is made to yield the pure difference spectra. Interestingly, approaches using specific kinetic models yield
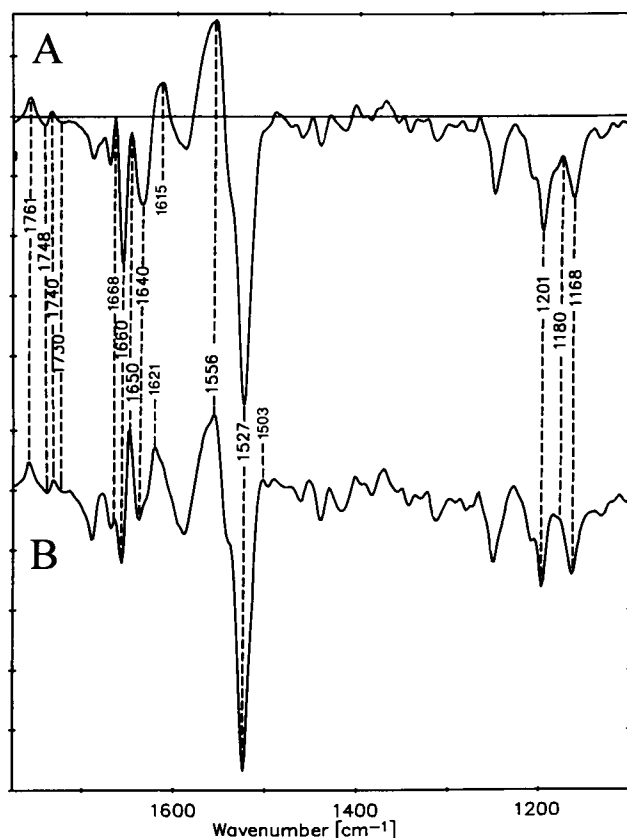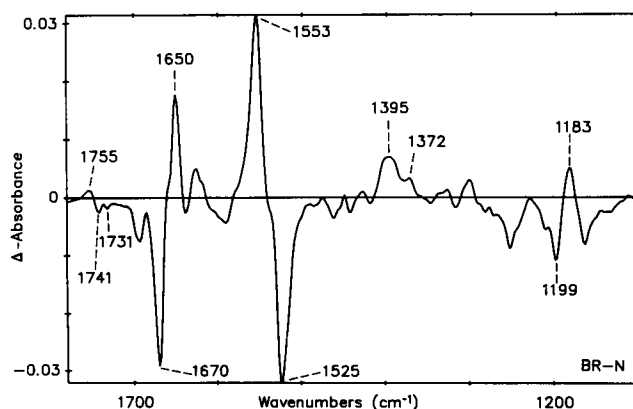


FIGURE 12   BR-N difference spectrum as obtained by factor analysis.

in general the same pure difference spectra in the visible as the approach performed here (Lozier et al., 1992; Váró and Lanyi, 1991a). The pure difference spectra in the infrared can be used as a reference for further studies—for example, with bacteriorhodopsin mutants and isotopically labeled bR. A comparison of the pure difference spectra with static difference spectra measured under unphysiological conditions (e.g., high pH or low temperature) now indicates which of them are useful. Furthermore, the comparison with amplitude spectra of time-resolved measurements indicates that under
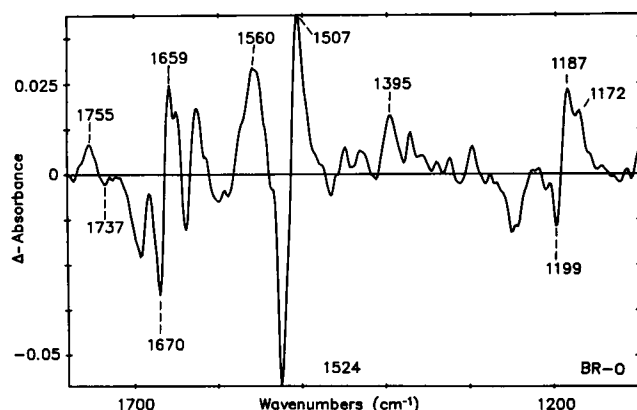
FIGURE 13   BR-O difference spectrum as obtained by factor analysis.

certain conditions just by global fitting almost pure spectra can be obtained.

From the time course of the intermediate concentrations in Fig. 9 it becomes clear that

1. Time-resolved measured difference spectra have more or less contributions of L also at later times of the photocycle in agreement with Ames and Mathies (1990).

2. Pure, physiologically relevant M spectra cannot be observed directly or as photostationary accumulated data due to overlap with L, N, and O intermediates.

3. At pH 6.5, the intermediate O accumulates, but the intermediate N still contributes significantly to O.

4. At pH 7.5, the intermediate N is kinetically separated from M and an almost pure N can be obtained, since the intermediate O contributes very little.

From the pure infrared difference spectra the following conclusions are drawn.

## BR-L

The comparison of BR-L difference spectra in the infrared measured at low and room temperature in Fig. 11 indicates different band patterns of protein vibrations but similar chromophore bands. The protein backbone bands (around 1660 $cm^{-1}$ and above), proline bands (1478/1468 $cm^{-1}$), and tyr 185 bands (1277 $cm^{-1}$) show different behavior (Braiman et al., 1988; Gerwert et al., 1990; Bousche et al., 1991). Most interestingly, the difference band (1742/1748 $cm^{-1}$) due to the asp 96 environmental shift at low temperature (Gerwert et al., 1989) is no longer clearly seen; only a negative band at 1742 $cm^{-1}$ and a new positive band at 1396 $cm^{-1}$ in the carboxylate region are visible (Engelhard et al., 1985; Braiman et al., 1991). Further experiments with asp-96 and asp-115 mutants are necessary to clarify whether this represents partial asp-96 deprotonation at room temperature in contrast to low temperature (Gerwert et al., 1989; Braiman et al., 1991; Rothschild, 1992). In summary, the results indicate clearly the importance of L measurements at room temperature because at low temperature a different protein state is stabilized. The different difference spectra may also indicate two different L intermediates.

## BR-M

In the literature, the presented BR-M difference spectra in the infrared spectral region (Engelhard et al., 1985; Braiman et al., 1988, 1991; Gerwert et al., 1989; Ormos, 1991; Ormos et al., 1992; Fahmy et al., 1992; Maeda et al., 1992; Perkins et al., 1993) show impurities due to L, N, and/or O contributions, respectively, as now quantified by factor analysis. Good indicators are the bands at 1755 $cm^{-1}$ and 1188 $cm^{-1}$. The time course of the intermediate concentrations in Fig. 9 show clearly that the time-resolved difference spectra measured during M formation or photostationary accumulated M cannot be used directly as pure BR-M difference spectra. By factor analysis and decomposition we are now able to extract one pure BR-M difference spectrum of physiological relevance. Conceptually, two different M intermediates are expected, one oriented with Schiff base toward the proton release pathway and one oriented toward the proton uptake pathway (Schulten and Tavan, 1978; Gerwert and Siebert, 1986; Lanyi, 1992; Oesterhelt et al., 1992). Different BR-M difference spectra presented up to now in the infrared are caused by impurities and are not due to the two different M intermediates (Ormos, 1991; Perkins et al., 1992). Low-temperature BR-M difference spectra shown by Souvignier and Gerwert (1992) and Ormos et al. (1992) deviate in the amide I region from factor analysis BR-M. But in the time-resolved series of difference spectra measured during the L to M to N reaction pathway at room temperature, such a difference spectrum is not observed. This calls into question its physiological relevance. A second M (called Mn) is detected at pH 10 in the asp-96-asn mutant (Sasaki et al., 1992), but it is unclear whether this represents the second wild-type M that we are searching for.

Even though factor analysis gives no direct indication for two different M intermediates, one M may be kinetically or spectrally merged with another intermediate and therefore not be observed. It is clear that the four basic difference spectra yielded by factor analysis do not fully describe the absorbance changes during the photocycle. The small apparent rates $k_5$ and $k_6$ obtained in global fitting are not reflected in the pure intermediate spectra. Because the two apparent rates describe biphasic M rise and decay, respectively, they might be caused by a second M that is not clearly separated kinetically or spectrally. It appears that under physiological conditions this second M cannot clearly be resolved in wild-type bacteriorhodopsin, and it is questionable whether it will be fully resolved with increased time resolution or increased $S/N$ ratio. The small deviations in the decay kinetics at pH 7.5 between the absorbance change at 410 nm and the time course of the M concentrations and the small amplitude at 410 nm in the pure BR-N difference spectrum may indicate that the BR-M difference spectrum extracted by factor analysis represents an early M, whereas a later, second M is merged with N. Nevertheless, an M1 to M2 transition might be better observed with slowed-down M-decay. The global fit analysis of the M decay at 220 K resolves two different rates. The amplitude spectrum of the

faster rate is almost identical to the BR-M difference spectum obtained by factor analysis. The amplitude spectrum of the slower rate shown in Fig. 11 *B* also represents a BR-M difference spectrum. In the earlier approaches these two spectra are merged into one (Ormos et al., 1992; Perkins et al., 1992). They deviate in the amide I region at 1668 cm$^{-1}$ and 1650 cm$^{-1}$ and in the amide II region at 1553/1527 cm$^{-1}$, indicating different protein backbone structures. This result supports a model in which a protein movement after M formation contributes to the orientation of the central proton binding site away from asp-85 and toward asp-96. But deviations in the fingerprint region at 1180 cm$^{-1}$ also indicate different chromophore configurations in the two M, supporting the hypothesis that the chromophore contributes to this movement, in contrast to a pure C-T model (Schulten and Tavan, 1978; Fodor et al., 1988). Double-flash experiments seem to be a promising method of resolving the problem of different M intermediates (Druckmann et al., 1992).

In summary: the pure BR-M difference spectrum most likely represents an early M. It indicates the protonation of asp-85 at 1762 cm$^{-1}$. The band pattern around 1732 cm$^{-1}$ now clearly resolved in the M-spectrum does not indicate asp-212 protonation (Fahmy et al., 1993). Unpublished results indicate a composition of asp-115 and asp-96 differential bands (Gerwert et al., manuscript in preparation).

## BR-N

The BR-N difference spectrum yielded by factor analysis agrees nicely with the amplitude spectrum of $k_6$ (Fig. 6 *f*). Because at pH 7.5 the N is kinetically well separated from M decay (Fig. 9, *bottom*), the apparent rate amplitude already describes a pure BR-N, as the factor analysis proves now. Furthermore, the factor analysis BR-N agrees with the BR-N measured at pH 10 (Pfefferlé et al., 1991), also supporting its relevance.

The following conclusions can be drawn from the pure BR-N difference spectrum:

1. asp-96 deprotonates not only at high pH but also under physiological conditions, as indicated by the negative band at 1742 cm$^{-1}$ (Gerwert et al., 1989, 1990b; Bousche et al., 1991; Maeda et al., 1992).

2. The asp-85 carbonyl frequency is shifted from 1762 cm$^{-1}$ in M to 1755 cm$^{-1}$ in N, indicating movement to a more hydrophilic environment (Braiman et al., 1991; Fahmy et al., 1992). It is also clear now that shoulders observed at 1755 cm$^{-1}$ in static "BR-M" difference spectra represent impurities due to N or O contributions.

3. The most prominent feature is the strong difference band at 1670/1650 cm$^{-1}$. These difference bands reflect a backbone movement of a few peptide carbonyl groups. It may represent the same structural change observed in time-resolved x-ray structure analysis (Koch et al., 1991) and in electron microscopy studies (Subramanian et al., 1993). In these studies the M to N reaction is not resolved and the reaction seems to appear in M. From factor analysis it is clear now that the main helical movement takes place after M

formation in the M to N transition or as discussed above in an unresolved $M_1$ to $M_2$ transition, in agreement with earlier conclusions (Gerwert et al., 1990b; Braiman et al., 1991; Ormos, 1991; Souvignier and Gerwert, 1992; Sasaki et al., 1992). It seems that the structural movement precedes asp-96 deprotonation, because the difference bands at 1670/1650 cm$^{-1}$ are already seen in the late BR-M amplitude spectrum (Fig. 11 *b*). An involvement of the structural movement in asp-96 pK reduction is also proposed by Sasaki et al. (1992).

## BR-O

The BR-O difference spectrum, which is not observable in its pure form directly, is clearly elucidated for the first time by factor analysis. The time-resolved series of difference spectra contain significant M and N contributions, even though O accumulates. Indicative O features are the chromophore bands at 1508 cm$^{-1}$ and 1172 cm$^{-1}$. The following conclusions are drawn from the BR-O difference spectrum:

1. asp-85 is still protonated in O, in agreement with earlier conclusions based on global fit analysis (Souvignier and Gerwert, 1992). The carbonyl band at 1755 cm$^{-1}$ is significantly increased in O as compared to N because its intensity is partially compensated in N by the disappearing asp-96 carbonyl vibration at 1742 cm$^{-1}$.

2. asp-96 is already reprotonated in O, which is in agreement with the results of our global fit analysis (Souvignier and Gerwert, 1992) because the factor analysis clearly shows no negative band at 1742 cm$^{-1}$ in O. asp-85 is protonated in N and O and therefore could not affect the absorption maximum. Asp-96, on the other hand, is deprotonated in N and reprotonated in O. Therefore it is appealing to assume that asp-96 controls the absorption maximum in N by stabilizing the positive chromophore charge at the Schiff base. Electrostatic interaction over 10 Å between asp-96 and the Schiff base is conceivable (Bashford and Gerwert, 1992). Nevertheless, on the other hand similiar shifts are observed in the asp-96-asn mutant lacking a negative charge. But in the mutant a different charge stabilization mechanism in N is likely.

3. A new carbonyl band appears at 1737 cm$^{-1}$, which is tentatively assigned to asp-115 carbonyl vibration undergoing an environmental change in O similar to the one in K.

4. The structural backbone change as indicated by the difference bands at 1670/1650 cm$^{-1}$ and 1560 cm$^{-1}$ is still present in O. The band at 1659 cm$^{-1}$ cannot represent the C=N vibration. It is observed at 1628 cm$^{-1}$ (Smith et al., 1983).

In the tyr-185-phe mutant an O-like intermediate is accumulated (Bousche et al., 1992). The mutant O-like difference spectrum also shows the O characteristic bands but in different relative intensities as compared to the pure wild-type O difference spectrum. As in the wild type, asp-96 is reprotonated in O and asp-85 is protonated. In contrast, the amide I difference band and therefore the protein backbone motion are already relaxed in the mutant in O. This may be due to a different mechanism in the mutant or may reflect two different O intermediates.
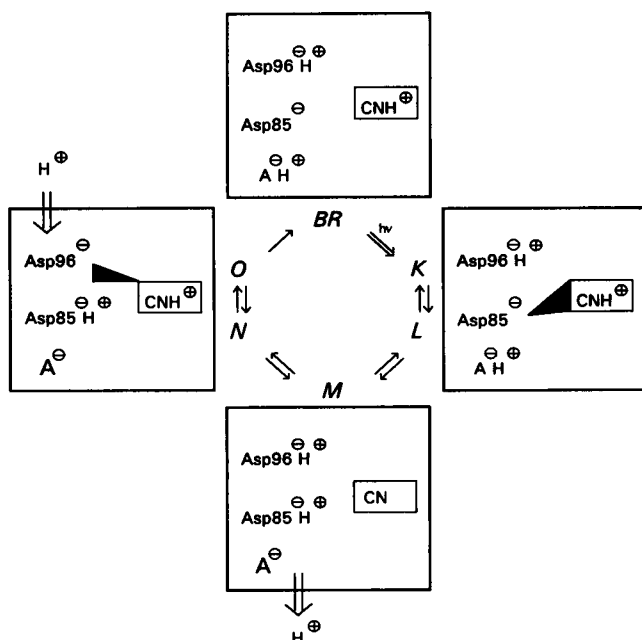
FIGURE 14 Basic four step scheme. The light-induced conformational change (retinal isomerization) orients in intermediates K and L the central proton binding site (CNH) to the protonrelease groups (asp 85, AH) resulting in proton release in intermediate M; the second conformational change (peptide C=O group motion) facilitates proton transfer between asp 96 and the Schiff base in N resulting in proton uptake. asp 96 is already reprotonated in O. Asp 85 reprotonates A⁻ in the O to BR reaction.

## CONCLUSION

Factor analysis and deconvolution yield, independently of specific kinetic models, the four basic difference spectra describing the intramolecular reactions during bacteriorhodopsin pump activity. The intramolecular reactions are assigned unequivocally to specific photocycle intermediates even if they overlap kinetically. The results confirm now in a clearcut manner the model proposed earlier based on a global fit analysis in all details (Fig. 12 in Souvignier and Gerwert, 1992; Gerwert, 1992) and are summarized in Fig. 14.

## REFERENCES

Ames, J. B., and R. A. Mathies. 1990. The role of back-reactions and proton uptake during N→O transition in bacteriorhodopsin's photocycle: a kinetic resonance Raman study. Biochemistry. 29:7181–7190

Bashford, D., and K. Gerwert. 1992. Electrostatic calculations of the pKa's of ionizable groups in bacteriorhodopsin. J. Mol. Biol. 224:473–486.

Bousche, O., M. Braiman, Y-W. He, T. Marti, H. G. Khorana, and K. J. Rothschild. 1991. Vibrational spectroscopy of bacteriorhodopsin mutants. J. Biol. Chem. 266:11063–11067.

Bousche, O., S. Sonar, M. Krebs, H. G. Khorana, and K. J. Rothschild. 1992. Time-resolved Fourier transform infrared spectroscopy of the bacteriorhodopsin mutant tyr185 phe, asp96 reprotonates during O formation; asp85 and asp212 deprotonate during O decay. Photochem. Photobiol. 267:1615–1622.

Braiman, M. S., T. Mogi, L. J. Stern, N. R. Hackett, B. H. Chao, H. G. Khorana, and K. J. Rothschild. 1988. Proteins Struct. Funct. Genet. 3:219–229.

Braiman, M. S., O. Bousché, and K. J. Rothschild. 1991. Protein dynamics in the bacteriorhodopsin photocycle submillisecond Fourier transform infrared spectra of the L, M, and N photointermediates. Proc. Natl. Acad. Sci. USA. 88:2388–2392.

Chen, W. G., and M. S. Braiman. 1991. Kinetic analysis of time-resolved infrared difference spectra of the L and M intermediates of bacteriorhodopsin. Photochem. Photobiol. 54:905–910.

Chernavskii, D. S., V. Chizhov, R. H. Lozier, T. M. Murina, A. M. Prokhorov, and B. V. Zubov. 1989. Kinetic model of bacteriorhodopsin photocycle: pathway from M state to bR. Photochem. Photobiol. 49:649–653.

Dancsházy, Zs., R. Govindjee, and T. G. Ebrey. 1988. Independent photocycles of the spectrally distinct forms of bacteriorhodopsin. Proc. Natl. Acad. Sci. USA. 85:6358–6361.

Diller, R., and M. Stockburger. 1988. Kinetic resonance Raman studies reveal different conformational states of bacteriorhodopsin. Biochemistry. 27:7641–7751.

Druckmann, S., N. Friedman, J. K. Lanyi, R. Needleman, M. Ottolenghi, and M. Sheves. 1992. The back photoreaction of the M intermediate in the photocycle of bacteriorhodopsin: mechanism and evidence for two M species. Photochem. Photobiol. 56:1041–1047.

Engelhard, M., K. Gerwert, B. Hess, W. Kreutz, and F. Siebert. 1985. Light-driven protonation of internal aspartic acids of bacteriorhodopsin: an investigation by static and time-resolved infrared difference spectroscopy using [4-¹³C] aspartic acid labeled purple membrane. Biochemistry. 24:400–407.

Fahmy, K., O. Weidlich, M. Engelhard, J. Tittor, D. Oesterhelt, and F. Siebert. 1992. Identification of the proton acceptor of Schiff base deprotonation in bacteriorhodopsin: a Fourier transform infrared study of the mutant asp 85 Glu in its natural lipid environment. Photochem. Photobiol. 56:1073–1083.

Fahmy, K., O. Weidlich, M. Engelhard, H. Sigrist, and F. Siebert. 1993. Aspartic acid-212 of bacteriorhodopsin is ionized in the M and N photocycle intermediates: an FTIR study on specifically 13-C-labeled reconstituted purple membranes. Biochemistry. 32:5862–5869.

Fodor, S. P. A., J. B. Ames, R. Gebhard, E. M. M. van den Berg, W. Stoeckenius, J. Lugtenburg, and R. A. Mathies. 1988. Chromophore structure in bacteriorhodopsin's N intermediate: implications for the proton-pumping mechanism. Biochemistry. 27:7097–7101.

Gerwert, K., and F. Siebert. 1986. Evidence for light-induced 13-cis, 14-s-cis isomerization in bacteriorhodopsin obtained by FTIR difference spectroscopy using isotopically labelled retinals. EMBO J. 5:805–811.

Gerwert, K., B. Hess, J. Soppa, and D. Oesterhelt. 1989. The role of Asp 96 in the proton pump mechanism of bacteriorhodopsin. Proc. Natl. Acad. Sci. USA. 86:4943–4947.

Gerwert, K., B. Hess, and M. Engelhard. 1990a. Proline residues undergo structural changes during proton pumping in bacteriorhodopsin. FEBS Lett. 261:449–459.

Gerwert, K., G. Souvignier, and B. Hess. 1990b. Simultaneous monitoring of light-induced changes in protein side-group protonation, chromophore isomerization and backbone motion of bacteriorhodopsin by time-resolved Fourier-transform infrared spectroscopy. Proc. Natl. Acad. Sci. USA. 87:9774–9778.

Gerwert, K. 1992. Molecular reaction mechanisms of photosynthetic proteins as determined by FTIR spectroscopy. Biochim. Biophys. Acta. 1101: 147–153.

Hanamoto, J. H., P. Dupuis, and M. A. El-Sayed. 1984. On the protein (tyrosine)-chromophore (protonated Schiff base) coupling in bacteriorhodopsin. Proc. Natl. Acad. Sci. USA. 81:7083–7087.

Henry, E. R., and J. Hofrichter. 1992. Singular value decomposition: application to analysis of experimental data. Methods Enzymol. 210: 129–192.

Heßling, B., G. Souvignier, and K. Gerwert. 1992. A new approach to analyse kinetic data of bacteriorhodopsin, factor analysis and decomposition. In Structures and Functions of Retinal Proteins. J. L. Rigaud, editor. Colloque INSERM/John Libbey Eurotex Ltd. 221:155–158.

Hofrichter J., E. R. Henry, and R. H. Lozier. 1989. Photocycles of bacteriorhodopsin in light- and dark-adapted purple membranes studied by time-resolved absorption spectroscopy. Biophys. J. 56:693–706.

Koch, M. H. J., N. A. Dencher, D. Oesterhelt, H-J. Plöhn, G. Rapp, and G. Büldt. 1991. Time-resolved x-ray diffraction study of structural changes associated with the photocycle of bacteriorhodopsiin. *EMBO J.* 10: 521–526.

Kouyama, T., A. Nasuda-Kouyama, A. Ikegami, M. K. Mathew, and W. Stoeckenius. 1988. Bacteriorhodopsin photoreaction: identification of a long-lived intermediate N/P R350 at high pH and its M-like photoproduct. *Biochemistry.* 27:5855–5863.

Lanyi, J. K. 1992. Proton transfer and energy coupling in the bacteriorhodopsin photocycle. *J. Bioenerg. Biomembr.* 24:169–179.

Lozier, R. H., R. A. Bogomolni, and W. Stoeckenius. 1975. Bacteriorhodopsin: a light-driven proton pump in *Halobacterium halobium.* *Biophys. J.* 15:955–962.

Lozier, R. H., A. Xie, J. Hofrichter, and G. M. Clore. 1992. Reversible steps in the bacteriorhodopsin photocycle. *Proc. Natl. Acad. Sci. USA.* 89: 3610–3614.

Maeda, A., J. Sasaki, Y. Shichida, T. Yoshizawa, M. Chang, B. Ni, R. Needleman, and J. K. Lanyi. 1992. Structures of aspartic acid-96 in the L and M intermediates of bacteriorhodopsin: analysis by Fourier transform infrared spectroscopy. *Biochemistry.* 31:4685–4690.

Malinowski, E. R. 1980. Factor Analysis in Chemistry. John Wiley and Sons, Ltd., New York.

Oesterhelt, D., J. Tittor, and E. Bamberg. 1992. A unifying concept for ion translocation by retinal proteins. *J. Bioenerg. Biomembr.* 24:181–191.

Ormos, P. 1991. Infrared spectroscopic demonstration of a conformational change in bacteriorhodopsin involved in proton pumping. *Proc. Natl. Acad. Sci. USA.* 88:473–477.

Ormos, P., K. Chu, and J. Mourant. 1992. Infrared study of the L, M, and N intermediates of bacteriorhodopsin using the photoreaction of M. *Biochemistry.* 31:693–6937.

Perkins, G. A., E. Liu, F. Burkard, E. A. Berry and R. M. Glaeser. 1992. Characterization of the conformational change in the $M_1$ and $M_2$ substates of bacteriorhodopsin by the combined use of visible and infrared spectroscopy. *J. Struct. Biol.* 109:142–151.

Pfefferlé, J. M., A. Maeda, J. Sasaki, and T. Yozikawa. 1991. Fourier transform infrared study of the N intermediate of bacteriorhodopsin. *Biochemistry.* 30:6548–6556.

Rothschild, K. J., Y.-W. He, T. Mogi, T. Marti, and H. G. Khorana. 1990. Vibrational spectroscopy of bacteriorhodopsin mutants: evidence for the interaction of proline-186 with the retinylidene chromophore. *Biochemistry.* 29:5954–5960.

Rothschild, J. R. 1992. FTIR difference spectroscopy of bacteriorhodopsin: toward a molecular model. *J. Bioenerg. Biomembr.* 24:147–166.

Sasaki, J., Y. Shichida, J. K. Lanyi and A. Maeda. 1992. Protein changes associated with reprotonation of the Schiff base in the photocycle of $Asp^{96} \rightarrow Asn$ bacteriorhodopsin. *J. Biol. Chem.* 267:20782–20786.

Schulten, K., and P. Tavan. 1978. A mechanism for the light-driven proton pump of *Halobacterium halobium.* *Nature (Lond.).* 272:85–86.

Smith, S. O., J. A. Pardoen, P. P. J. Mulder, B. Curry, J. Lugtenburg, and R. Mathies. 1983. Chromophore structure in bacteriorhodopsin's $O_{640}$ photointermediate. *Biochemistry.* 22:6141–6148.

Smith, S. O., A. B. Myers, J. A. Pardoen, C. Winkel, P. P. J. Mulder, J. Lugtenburg, and R. Mathies. 1984. Determination of retinal Schiff base configuration in bacteriorhodopsin. *Proc. Natl. Acad. Sci. USA.* 81: 2055–2059.

Souvignier, G., and K. Gerwert. 1992. Proton uptake mechanism of bacteriorhodopsin as determined by time-resolved stroboscopic-FTIR-spectroscopy. *Biophys. J.* 63:1393–1405.

Subramanian, S., M. Gerstein, D. Oesterhelt, and R. Henderson. 1993. Electron diffraction analysis of structural changes in the photocycle of bacteriorhodopsin. *EMBO J.* 12:1–8.

Váró, G., and L. Lanyi. 1990. Pathways of the rise, and decay of the M photointermediate(s) of bacteriorhodopsin. *Biochemistry.* 29:2241–2250.

Váró, G., and J. K. Lanyi. 1991a. Distortions in the photocycle of bacteriorhodopsin at moderate dehydration. *Biophys. J.* 59:313–322.

Váró, G., and J. K. Lanyi. 1991b. Kinetic and spectroscopic evidence for an irreversible step between deprotonation and reprotonation of the Schiff base in the bacteriorhodopsin photocycle. *Biochemistry.* 30:5008–5015.

Váró, G., and J. K. Lanyi. 1991c. Thermodynamics and energy coupling in the bacteriorhodopsin photocycle. *Biochemistry.* 30:5016–5022.

Xie, A. H., J. F. Nagle, and R. H. Lozier. 1987. Flash spectroscopy of purple membrane. *Biophys. J.* 51:627–635.

Zimanyi, L. and J. K. Lanyi. 1993. Deriving the intermediate spectra and photocycle kinetics from time-resolved difference spectra of bacteriorhodopsin. *Biophys. J.* 64:240–251.

Zundel, G. 1988. Proton transfer in an proton polarizability of hydrogen bonds: IR and theoretical studies regarding mechanisms in biological systems. *J. Mol. Struct.* 177:43–68.